Geophysical Research Letters

RESEARCH LETTER
10.1029/2021GL094551

EC-Earth Simulations Reveal Enhanced Inter-Hemispheric Thermal Contrast During the Last Interglacial Further Intensified the Indian Monsoon

Kaiqi Chen[1], Josefine Axelsson[2], Qiong Zhang[2], Jianping Li[3,4], and Lanning Wang[1]

[1]College of Global Change and Earth System Sciences, Beijing Normal University, Beijing, China, [2]Department of Physical Geography and Bolin Centre for Climate Research, Stockholm University, Stockholm, Sweden, [3]Frontiers Science Center for Deep Ocean Multispheres and Earth System (FDOMES)/Key Laboratory of Physical Oceanography/Institute for Advanced Ocean Studies, Ocean University of China, Qingdao, China, [4]Laboratory for Ocean Dynamics and Climate, Pilot Qingdao National Laboratory for Marine Science and Technology, Qingdao, China

Abstract Paleoclimate proxy data indicate a stronger Indian summer monsoon (ISM) during the Last Interglacial (LIG) than in the present day. This is largely attributed to orbital forcing induced high seasonal and latitudinal insolation anomalies in the Northern Hemisphere during LIG. According to the general circulation model EC-Earth3, the simulated ISM rainfall is increased by approximately 28% during the LIG compared to the pre-industrial period as a result of the orbital forcing and the amplified land-sea contrast due to both local and remote ocean feedbacks. Although the LIG is often portrayed as a potential analogue of future warmer climates, our study suggests that the enhanced inter-hemispheric thermal gradient during the LIG strengthened the ISM, in opposition to the observed weakening of ISM under present-day warming.

Plain Language Summary One way to understand the future climate change is to learn from the past warm periods. The period of the Last Interglacial (LIG) is often referred to as a potential analogue for what a future climate may look like. However, paleoclimate archives such as speleothems show a stronger Indian summer monsoon (ISM) during the LIG, in contrast to an observed weakening trend in ISM in the past century. In this study, we use the climate model simulations from EC-Earth3 to explain why the opposite changes happened in ISM during LIG and the current global warming period. The warming in the LIG was caused by a changed distribution of solar radiation over the Earth; in contrast, the current warming results from increased greenhouse gas concentrations in the atmosphere. The changes in the ISM are mainly determined by the thermal differences between land and ocean in the region. Due to its special geographical location, that is, the north-south orientation of land and ocean, the solar radiation changes in the LIG enhanced the land-sea temperature gradient, and thus intensified the ISM. Therefore, the response in the ISM to the present-day warming climate is different from that to the warm LIG climate.

Key Points:

- The EC-Earth model simulations demonstrate a 28% increase in Indian summer monsoon rainfall during the Last Interglacial (LIG)
- Orbital forcing in the LIG increased the inter-hemispheric thermal gradient and enhanced the land-sea contrast in South Asia
- The Indian summer monsoon during the LIG was further amplified by feedbacks in the equatorial Indian Ocean and Pacific Ocean

Correspondence to:

Q. Zhang and J. Li,
qiong.zhang@natgeo.su.se;
ljp@ouc.edu.cn

Citation:

Chen, K., Axelsson, J., Zhang, Q., Li, J., & Wang, L. (2022). EC-Earth simulations reveal enhanced inter-hemispheric thermal contrast during the Last Interglacial further intensified the Indian monsoon. *Geophysical Research Letters*, *49*, e2021GL094551. https://doi.org/10.1029/2021GL094551

Received 3 JUN 2021
Accepted 3 MAR 2022

Author Contributions:

Conceptualization: Kaiqi Chen, Josefine Axelsson, Qiong Zhang
Data curation: Qiong Zhang
Formal analysis: Kaiqi Chen
Funding acquisition: Qiong Zhang, Jianping Li, Lanning Wang
Methodology: Kaiqi Chen, Josefine Axelsson
Visualization: Kaiqi Chen
Writing – original draft: Kaiqi Chen, Josefine Axelsson, Qiong Zhang
Writing – review & editing: Kaiqi Chen, Josefine Axelsson, Qiong Zhang

1. Introduction

As one of the most powerful tropical monsoon climate systems in the world, the Indian summer monsoon (ISM) can bring moisture from the Indian Ocean toward the continent, resulting in heavy precipitation (Buckley et al., 2014). Even small changes in precipitation over the Indian subcontinent could have significant consequences for agricultural production and socio-economic development (Gadgil & Kumar, 2006; Singh et al., 2014; Vittal et al., 2020). Model results have shown that changes to the ISM are highly sensitive to global warming (Kitoh et al., 2013). Although the frequency and intensity of extreme rain events over India have increased over the past century, seasonal mean rainfall has rather decreased (Goswami et al., 2006; Roxy et al., 2015). Meanwhile, both model simulations and observations indicate that global warming has caused sea surface temperature (SST) in the tropical eastern Indian Ocean to rise, which has resulted in a weakening of the land-sea thermal gradient and reduced ISM precipitation (Dinezio et al., 2020; Ramesh & Goswami, 2007; Roxy et al., 2015). Climate models participating in the Fifth Climate Model Intercomparison Project (CMIP5) show a large uncertainty in their projections of the Indian monsoon system (Saha et al., 2014). It has been suggested that past warm climates could be used as a potential analogue to understand future climate changes. As part of CMIP, the Paleoclimate Model Intercomparison Project (PMIP) plays an important role in evaluating the ability of CMIP6 models to reproduce past climates by comparing with paleoclimate proxy-data records and to further our understanding

of regional responses to a warmer climate, such as changes in the Indian monsoon (Harrison et al., 2015; Hirabayashi et al., 2013).

The most recent warm period is the Last Interglacial (LIG), which lasted from 129 to 116 thousand years (ka) before the present. During the LIG, the geographical setting and concentration of greenhouse gases (GHGs) in the atmosphere were almost comparable to pre-industrial levels. The main difference was the incoming solar radiation caused by changes in the Earth's orbit. The reconstructions of global mean SST during LIG were ~2°C higher than modern observations (Hoffman et al., 2017), and SST in the northern middle and high latitudes were up to 3.8°C higher (Turney et al., 2020). These global and hemispheric warming features are similar to projections of future global warming (Otto-Bliesner et al., 2017). The signal of long-term precipitation changes in the Indian monsoon has been mostly recorded in marine sediments and cave deposits such as stalagmites (Cai et al., 2015; Cheng et al., 2016; Midhun et al., 2018). The $\delta^{18}O$ signal recorded in stalagmites is one of the most important water tracers, but it has given conflicting results regarding changes in Asian monsoon precipitation (Y. Wang et al., 2008b; Zhang & Chen, 2020). Previous studies have combined stalagmite $\delta^{18}O$, $\delta^{44}Ca$, and elemental ratios (e.g., Mg/Ca, Sr/Ca, and Ba/Ca) and shown that the ISM was unstable during the LIG period (Magiera et al., 2019). One reason for this is that the variation in $\delta^{18}O$ is affected more by large-scale atmospheric dynamics than by regional precipitation (Li, 2018; Tan, 2014). However, stalagmite records from India indicate that South Asia was wetter during the LIG than in the preindustrial (PI) period, and proxy-record evidence of increased monsoon precipitation has also been found for the East Asian summer monsoon. This suggests that both monsoon systems have a high monsoonal activity during the peak of LIG, that is, at 127 ka (Liu et al., 2020; Scussolini et al., 2019).

The LIG has been one of the main target periods in PMIP since PMIP3 (Kageyama et al., 2018). The multi-model results and ensembles both show that there is significant warming in almost all continents during boreal summer with respect to the PI simulations of the same models (Lunt et al., 2013; Otto-Bliesner et al., 2021). The increased ISM precipitation observed from proxy records during the LIG contrasts with the decreased ISM precipitation projected under continuous global warming (Cheng et al., 2016; Turner & Annamalai, 2012). Scussolini et al. (2019) note that multi-model ensembles show that the significant increase of ISM precipitation during the LIG period is consistent with the increase of cloud cover and surface cooling. However, there is still a large gap in our understanding of the dynamics of ISM precipitation during the LIG period compared with the present (Han et al., 2019). Current global warming has provided an important impetus to study climatology at higher global temperatures.

Here we use simulations from the global coupled climate model EC-Earth3-LR to investigate climatic changes in the ISM region and the implications of orbital forcing by comparing LIG to a PI control experiment. Understanding the dynamics of ISM precipitation which is relevant to the inter-hemispheric temperature difference during the LIG will also provide a strong scientific basis for predicting spatiotemporal changes in the Indian climate.

2. Model Simulations and Methods

2.1. EC-Earth3-LR Model and Setup

In this study, we use the PMIP4/CMIP6 simulations of the LIG and PI period performed by EC-Earth3-LR (Zhang et al., 2021). EC-Earth is a fully coupled Earth system model that is developed by a European consortium of around 30 research institutions and is widely used in various studies on climate change (Hazeleger et al., 2010, 2012). The atmospheric component of EC-Earth3 is the Integrated Forecasting System model (cycle 36r4) of the European Center for Medium-Range Weather Forecasts (ECMWF), which contains the land surface Hydrology Tiled ECMWF Scheme for Surface Exchanges over Land (Balsamo et al., 2009). The ocean model is the Nucleus for European Modeling of the Ocean (NEMO) (Madec, 2008), coupled with the dynamic–thermodynamic sea-ice model Louvain-la-Neuve version 3 (LIM3) (Vancoppenolle et al., 2012). Atmospheric-land and ocean-sea-ice components are coupled through the Ocean, Atmosphere, Sea Ice, Soil coupler (Craig et al., 2017). The horizontal resolution of the atmosphere and land is 125 km with 62 vertical layers in the atmosphere; the ocean model, NEMO, has a horizontal resolution of 110 km with 75 vertical layers.

Through model intercomparisons, EC-Earth3-LR simulates a positive temperature bias in the Arctic region during LIG, hence a weaker boreal latitudinal temperature gradient compared to other PMIP4 model simulations, while the simulated southern hemisphere latitudinal temperature gradient is close to the PMIP4 ensemble

mean (Otto-Bliesner et al., 2021). Negative surface temperature responses in the Indian Monsoon region are similar in the range between EC-Earth3-LR and ensemble mean (Otto-Bliesner et al., 2021; Zhang et al., 2021). Global monsoons in the EC-Earth3-LR simulations have also been evaluated in Zhang et al. (2021) for mid-Holocene, LIG and mid-Pliocene. Changes relative to pre-industrial simulations have shown that the model changes in monsoon area and intensity in all three warming climates in relation to the forcing and the pre-industrial simulation.

We have run the LIG (lig127k) and PI (piControl) simulations following the PMIP4/CMIP6 protocol (Otto-Bliesner et al., 2017). The piControl and lig127k have the same boundary conditions except for the orbital forcing and GHGs. A detailed description of the piControl and lig127k simulations with EC-Earth3-LR is given in Zhang et al. (2021). The orbital forcing is calculated internally in the model. The CO_2, CH_4, and N_2O concentrations in the atmosphere are 284.3 ppm, 808.2 ppb, and 273 ppb in the piControl run and 275 ppb, 685 ppb, and 255 ppb in the lig127k run. The lig127k simulation starts from the pre-industrial initial conditions and has a spin-up time of about 300 years to reach equilibrium (i.e., when the global mean surface air temperature trend is less than 0.05 K per century). Here we present analysis based on the simulation 200 years post-equilibrium.

2.2. Calendar Adjustments

Changes in orbital configuration during the LIG resulted in a change in the month lengths (Bartlein & Shafer, 2019; Joussaume & Braconnot, 1997), and led to longer summers and shorter winters in Northern Hemisphere than during present-day and in the piControl simulation. We used the modern calendar for both the lig127k and the piControl experiment. To account for the impact that the changes in the length of months have on model output, we used the PaleoCalAdjust software (Bartlein & Shafer, 2019) on the simulation data from the lig127k experiment.

2.3. Statistical Methods and Indices

To investigate changes to the ISM during the LIG, we use a unified dynamical normalized seasonality (DNS) monsoon index defined by Li & Zeng (2002). This index represents the intensity of the monsoon based on the wind field rather than precipitation. It has been shown that this index has a solid dynamics basis and represents the seasonal cycle and interannual variability of the monsoon over various areas well, especially in Asia (Wang et al., 2008a). The index has also been adopted by the National Oceanic and Atmospheric Administration (https://www.cpc.ncep.noaa.gov/products/Global_Monsoons/Asian_Monsoons/Figures/Index/).

We compute the DNS monsoon index using the monthly mean wind field at 850 hPa from the PI control and lig127k simulations.

The DNS index δ is given by

$$\delta = \frac{||\overline{\boldsymbol{V}}_1 - \boldsymbol{V}_{n,m}||}{||\overline{\boldsymbol{V}}||} - 2, \tag{1}$$

where $\overline{\boldsymbol{V}}_1$ and $\overline{\boldsymbol{V}}$ are the wind vectors at a point for the climatological mean of January and the climatological mean of January and July, respectively. $\boldsymbol{V}_{nm}$ is the wind vectors in the mth month of the nth year. Note that 2 is subtracted from the right-hand side of the equation because the critical value of significance of the quantity $||\overline{\mathbf{V}}_1 - \mathbf{V}_7||/||\overline{\mathbf{V}}||$ is 2 (Li & Zeng, 2000). Two vertical bars (‖*‖) denote a norm on the monsoon domain of integration. Here, the Indian monsoon domain is defined as 5°–22.5°N and 35°–97.5°E. The norm ‖A‖ is defined as

$$||A|| = \left(\iint_S |\mathrm{A}|^2 \mathrm{dS} \right)^{1/2}, \tag{2}$$

where S denotes the domain of integration. In calculations at a point (i, j),

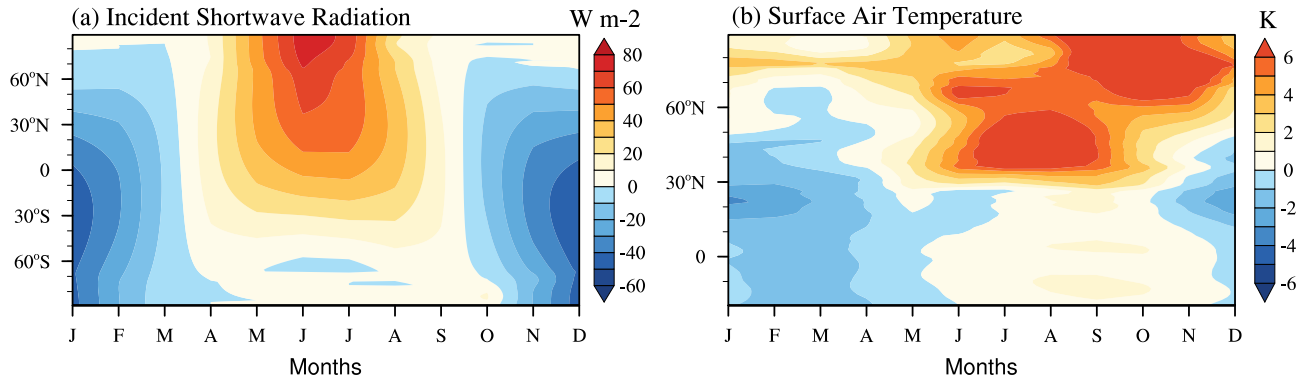

Figure 1. Differences between the Last Interglacial and preindustrial periods (lig127k minus piControl, the same in other figures) in (a) insolation at the top of the atmosphere and (b) surface air temperature, averaged over 50°–100°E.

$$||A_{i,j}|| \approx \Delta S[(|A^2_{i-1,j}| + 4|A^2_{i,j}| + |A^2_{i+1,j}|)\cos\varphi_j^{1/2} + |A^2_{i,j-1}|\cos\varphi_{j-1} + |A^2_{i,j+1}|\cos\varphi_{j+1}], \quad (3)$$

where $\Delta S = a\Delta\varphi\Delta\lambda/4$, φ_j is the latitude at the point (i, j), $\Delta\varphi$ and $\Delta\lambda$ are resolutions in the meridional and zonal directions, respectively, and a is the mean radius of the Earth (Li & Zeng, 2000).

3. Enhanced Land–Sea Contrast and Changes in ISM Due To Orbital Forcing

Differences in the Earth's orbital parameters (the precession, obliquity, and eccentricity) during the LIG led to differences in the seasonal and latitudinal distribution of solar radiation received at the top of the atmosphere compared with PI conditions (Berger & Loutre, 1991; Otto-Bliesner et al., 2017; Yeung et al., 2021). In lig127k, the incoming solar radiation received by the Northern Hemisphere (calculated as the hemispheric mean over 0°–90°N) increased by 40 W/m^2 from June to September (JJAS), which is 10% more than that during the PI period (Figure 1a). The increase in insolation was larger in the Northern Hemisphere than in the Southern Hemisphere, leading to an even larger inter-hemispheric thermal gradient.

Increased solar radiation directly affects the amount of heat reaching the surface and changes the surface energy budget. With increased incoming solar radiation in summer, the amplified warming over land is larger than that over the ocean (Figure 1b) and this land-sea contrast triggers the onset of the monsoon. The orbital forcing induced surface warming over both land and ocean, but the warming amplitude was larger over the land than over the ocean (Figure 1b). The southernmost latitude of the Indian continent is about 9°N. The surface temperature of Western Asia (10°–40°N, 50°–100°E) increased by ∼2.2°C in JJAS, whereas the surface air temperature of the northern Indian Ocean (10°S–10°N and 50°–100°E) increased by only 0.6°C (Figure 1b). We calculate the land-sea contrast by taking the temperature difference between the continent of Western Asia and the northern Indian Ocean. The land-sea contrast in the PI period was 2.8°C over the Indian monsoon region, but during the LIG it was ∼1.3°C, that is, ∼45% larger. An increase in the land-sea thermal contrast should enhance monsoon and lead to more monsoon precipitation (Chou, 2003; Wu et al., 2012; Yeung et al., 2021), which previous studies have found over the Indian subcontinent during the LIG period (Magiera et al., 2019; Montoya et al., 2000).

We further quantify the differences in the intensity of the ISM between the LIG and PI periods using the DNS method proposed by Li & Zeng (2002). The DNS index indicates that the average intensity of the ISM during the LIG was ∼32% higher than during the PI period. Turner and Annamalai (2012) note that under current GHGs forcing, although the increased land-sea contrast and water vapor should theoretically exacerbate monsoon precipitation, observations contrarily suggests a negative trend. A series of climate model experiments have also simulated a decrease in ISM precipitation, accompanied by a weakening of the circulation during the 20th century, mainly attributed to human-influenced aerosol emissions (Bollasina et al., 2011; Roxy et al., 2015; Salzmann & Cherian, 2015; Salzmann et al., 2014). This phenomenon may be related to the complex dynamical feedbacks within the tropical Indo-Pacific region. In contrast, we found a significant increase of ∼28% in ISM

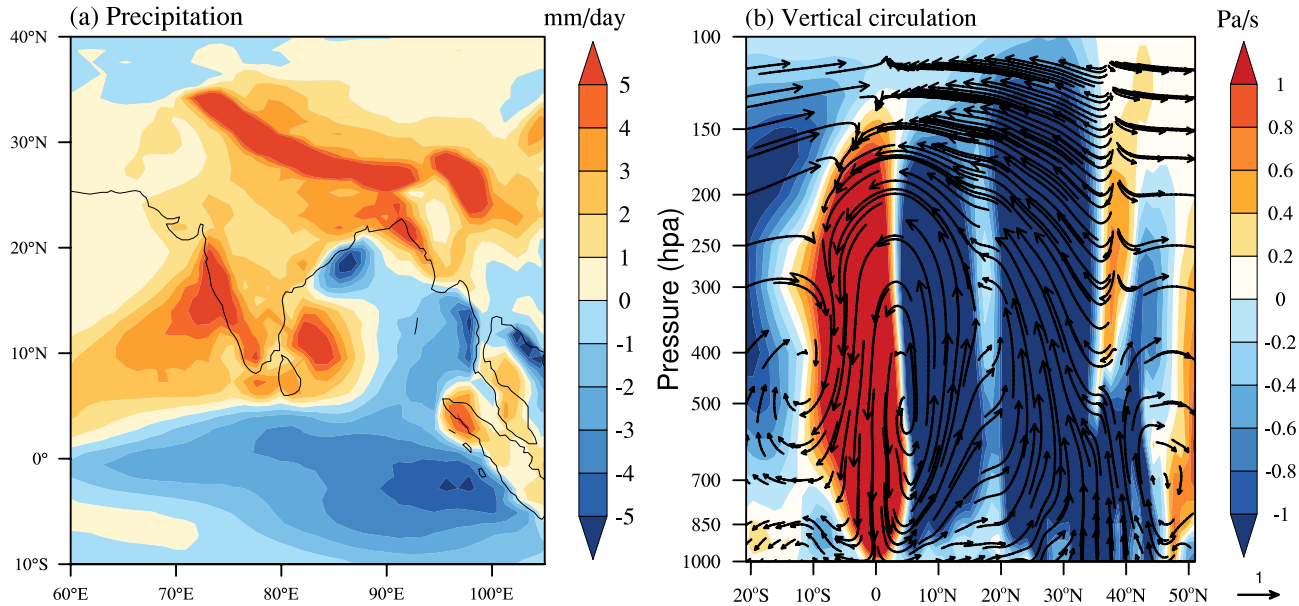

Figure 2. Differences between the Last Interglacial and preindustrial periods in June to September in (a) precipitation and (b) vertical circulation averaged over 60°–100°E.

precipitation during the LIG warm period compared to the PI period (Figure 2a). The major changes in precipitation were prominent in three areas: increased precipitation on the south side of the Himalayas, the west side of the Western Ghats, and reduced precipitation over the equatorial eastern Indian Ocean.

The comparison between the LIG and PI period shows that the changes in the vertical circulation in the Indian monsoon region (Figure 2b) correspond well to the changes in ISM Indian monsoon precipitation (Figure 2a). Two prominent local Hadley circulations resemble a "Double-Wall" structure. The ascending airflow near 10°N and 30°N is within the Indian subcontinent and corresponds to the high precipitation centers shown in Figure 2a. The descending branch is located in the equatorial region around 10°S–5°N and corresponds to the reduced precipitation in the equatorial eastern Indian Ocean in Figure 2a. This suggests that the monsoonal flow carried water vapor northward from the Indian Ocean, resulting in strong convection when the topographic barrier was reached. The relationship between the precipitation anomaly pattern and the topography emphasizes the influence of topography and the vertical atmospheric motion on precipitation (Bookhagen & Burbank, 2006; Sudharsan et al., 2020).

4. Ocean Feedbacks and Remote Forcing From the Pacific

Saji et al. (1999) showed that the tropical Indian Ocean SST has an important influence on the ISM. Figure 3 shows the correlation between the intensity of the ISM (as measured by the DNS time series index) and the tropical Indian Ocean SST in the LIG period. The conventional Indian monsoon index is primarily based on precipitation, whereas the DNS method, by taking the wind field into account, is more strongly grounded in atmospheric dynamics and describes regional circulations more clearly and accurately (Li et al., 2010; Zhang et al., 2018). Figure 3 shows that there was a statistically significant correlation between the equatorial Indian Ocean SST and the DNS index during the LIG. The correlation exhibits a dipole pattern, with negative correlations in the eastern part of the equatorial Indian Ocean and positive correlations in the western part.

This correlation pattern resembles the SST differences between the LIG and PI periods (Figure 4a). During the LIG, there was a cold tongue in the eastern equatorial Indian Ocean, with the largest part lying in the Southern Hemisphere. The increased insolation during the LIG (Figure 1a) did not prevent the formation of this cold tongue and the strong seasonal inter-hemispheric thermal contrast. As shown in Figure 4a, the anomalous easterly winds in the middle of the equatorial Indian Ocean were significantly stronger during the LIG than those in the PI period. Since the large-scale cooling in the equatorial Indian Ocean (Figure 4a) corresponds to the area with

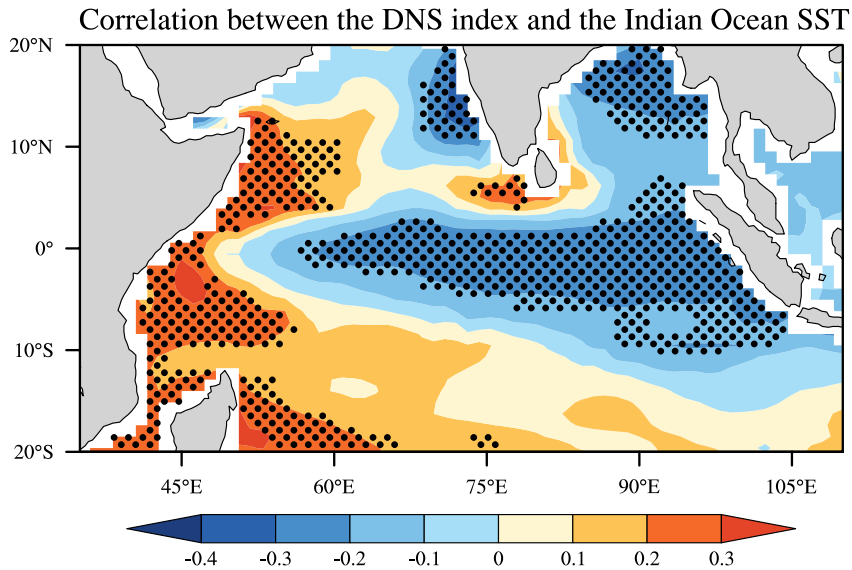

Figure 3. Correlation between the annual dynamical normalized seasonality index and the Indian Ocean sea surface temperature in June to September during the Last Interglacial period. The stippled area indicates statistical significance at the 0.05 level.

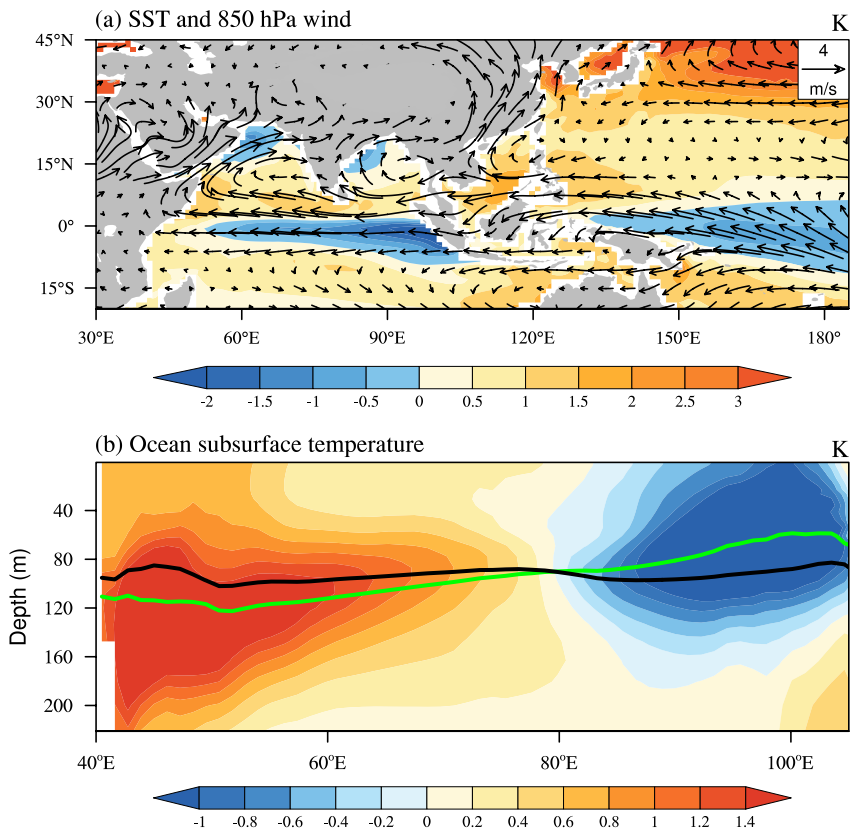

Figure 4. Differences in June to September-mean between the Last Interglacial (LIG) and preindustrial (PI) periods in (a) 850 hPa wind (vectors), sea surface temperature (shading), and (b) ocean subsurface temperature, averaged over 10°S–5°N. The green line in (b) indicates the thermocline represented by 23°C isotherm (Dinezio et al., 2020) during the LIG, and the black line indicates the thermocline in the PI period.

a negative correlation between the DNS index and JJAS SST (Figure 3), it indicates this cooling could be a main driver of the increase in ISM. Bollasina and Ming (2013) showed that the spatial expansion of the Indian Ocean SST mode can affect ocean convection through the modulation of the atmospheric meridional circulation. Such an SST pattern increased the meridional SST gradient in the equatorial Indian Ocean during the LIG. The air on the west side was warmed and rose, whereas on the east side it was cooled and sunk, thus strengthening the anomalous easterly winds at the surface of the equatorial Indian Ocean.

Furthermore, the Pacific Ocean can establish a connection with the tropical Indian Ocean through atmospheric circulation (Alexander et al., 2002; Terray et al., 2021; Tokinaga et al., 2012), which can contribute to the generation of anomalous easterly winds. In addition to the inter-hemispheric thermal contrast in the Indian Ocean in JJAS, there was a strong SST gradient between the northern and southern Pacific Ocean (Figure 4a). As the SST increased in the North Pacific, the air mass warmed and sunk over the cold SST in the South Pacific, creating a meridional Hadley Circulation over the Pacific Ocean (not shown). Due to the Coriolis force in the Southern Hemisphere, the downdrafts were deflected westward over the sea surface, forming anomalous easterly winds over the equatorial western Pacific and Indo-Pacific Warm Pool. According to the ocean-atmosphere coupling theory (Bjerknes, 1969), the upwelling of the equatorial eastern Indian Ocean was enhanced under the action of the anomalous easterly winds. As the thermocline became shallower (deeper) in the equatorial eastern (western) Indian Ocean, the SST formed a dipole of anomalies corresponding to the "warm West and cold East" pattern (Figure 4b). In addition, with the expansion of the SST cooling area in the equatorial eastern Indian Ocean, the land-sea thermal gradient in South Asia was further increased, which had a positive effect on the ISM precipitation.

5. Conclusions

The climate warming during the LIG was caused by different external forcing compared to present-day global warming. Anthropogenic GHGs emissions are the main forcing of current warming, whereas orbital forcing drove the inter-hemispheric thermal contrast during the LIG. Using the EC-Earth3-LR model, we explored the response in ISM to the LIG warm period compared to the PI. We found that the ISM was intensified during the LIG, resulting from enhanced inter-hemispheric thermal contrast due to direct response to insolation change and further amplified by local and remotely forced ocean mechanisms. Two anomalous meridional Hadley circulation structures were formed through topographic uplift, leading to increased precipitation on the coast of the Western Ghats and the south side of the Himalayas, and a significant decrease in precipitation was found in the equatorial eastern Indian Ocean. Furthermore, the inter-hemispheric thermal contrast formed anomalous easterly winds in the equatorial eastern Indian Ocean. A similar mechanism in the western Pacific resulted in anomalous easterly winds, which further enhanced the easterly winds in the eastern Indian Ocean. The weakened westerly winds led to a shallower thermocline in the equatorial eastern Indian Ocean and the subsequent upwelling enlarged the cooling area of the sea surface. A cooler eastern Indian Ocean further increased the thermal gradient between the Eurasian continent and the northern Indian Ocean, thus enhancing the ISM.

Unlike the weakening of the monsoon caused by present-day warming and aerosol emissions, the enhanced inter-hemispheric thermal contrast strengthened the ISM during the LIG. Therefore, we claim that LIG as a potential analogue for future warming does not hold for the ISM. This mechanism is specific to the Indian monsoon, where the land-sea contrast is in the north-south direction, and may not affect the West African monsoon or the East Asian monsoon, where the land-sea contrast is in the west-east direction. The mechanisms revealed behind the response of the ISM to orbital forcing during the LIG could offer a useful perspective to understand and interpret past and future climatic change in the ISM domain.

Data Availability Statement

The model simulations analysed in this study are distributed and made freely available through the Earth System Grid Federation (ESGF). The PI simulations are available at https://doi.org/10.22033/ESGF/CMIP6.4847 (EC-Earth Consortium (EC-Earth), 2019). The LIG simulations are available at https://doi.org/10.22033/ESGF/CMIP6.4798 (EC-Earth Consortium (EC-Earth), 2020).

Acknowledgments
The EC-Earth simulations were performed on ECMWF's computing and archive facilities. Additional resources were provided by the Swedish National Infrastructure for Computing (SNIC) at the National Supercomputer Centre (NSC) partially funded by the Swedish Research Council through grant agreement no. 2018–05913. We thank the two anonymous reviewers for their constructive inputs.

References

Alexander, M. A., Blade´, I., Newman, M., Lanzante, J. R., Lau, N. C., & Scott, J. D. (2002). The atmospheric bridge: The influence of ENSO teleconnections on air-sea interaction over the global oceans. *Journal of Climate*, *15*(16), 2205–2231. https://doi.org/10.1175/1520-0442(2002)015<2205:TABTIO>2.0.CO;2

Balsamo, G., Viterbo, P., Beljaars, A., van den Hurk, B., Hirschi, M., Betts, A. K., & Scipal, K. (2009). A revised hydrology for the ECMWF model: Verification from field site to terrestrial water storage and impact in the Integrated Forecast System. *Journal of Hydrometeorology*, *10*(3), 623–643. https://doi.org/10.1175/2008JHM1068.1

Bartlein, P. J., & Shafer, S. L. (2019). Paleo calendar-effect adjustments in time-slice and transient climate-model simulations (PaleoCalAdjust v1.0): Impact and strategies for data analysis. *Geoscientific Model Development*, *12*(9), 3889–3913. https://doi.org/10.5194/gmd-12-3889-2019

Berger, A., & Loutre, M.-F. (1991). Insolation values for the climate of the last 10 million years. *Quaternary Science Reviews*, *10*(4), 297–317. https://doi.org/10.1016/0277-3791(91)90033-Q

Bjerknes, J. (1969). Atmospheric teleconnections from the equatorial Pacific. *Monthly Weather Review*, *97*(3), 163–172. https://doi.org/10.1175/1520-0493(1969)097<0163:atftep>2.3.co;2

Bollasina, M. A., & Ming, Y. (2013). The general circulation model precipitation bias over the southwestern equatorial Indian Ocean and its implications for simulating the South Asian monsoon. *Climate Dynamics*, *40*(3), 823–838. https://doi.org/10.1007/s00382-012-1347-7

Bollasina, M. A., Ming, Y., & Ramaswamy, V. (2011). Anthropogenic aerosols and the weakening of the South Asian summer monsoon. *Science*, *334*(6055), 502–505. https://doi.org/10.1126/science.1204994

Bookhagen, B., & Burbank, D. W. (2006). Topography, relief, and TRMM-derived rainfall variations along the Himalaya. *Geophysical Research Letters*, *33*, L08405. https://doi.org/10.1029/2006GL026944

Buckley, B. M., Fletcher, R., Wang, S.-Y. S., Zottoli, B., & Pottier, C. (2014). Monsoon extremes and society over the past millennium on mainland Southeast Asia. *Quaternary Science Reviews*, *95*(7), 1–19. https://doi.org/10.1016/j.quascirev.2014.04.022

Cai, Y., Fung, I. Y., Edwards, R. L., An, Z., Cheng, H., Lee, J.-E., et al. (2015). Variability of stalagmite-inferred Indian monsoon precipitation over the past 252,000 y. *Proceedings of the National Academy of Sciences* 112(10), 2954–2959. https://doi.org/10.1073/pnas.1424035112

Cheng, H., Edwards, R. L., Sinha, A., Spötl, C., Yi, L., Chen, S., et al. (2016). The Asian monsoon over the past 640,000 years and ice age terminations. *Nature*, *534*(7609), 640–646. https://doi.org/10.1038/nature18591

Chou, C. (2003). Land–sea heating contrast in an idealized Asian summer monsoon. *Climate Dynamics*, *21*(1), 11–25. https://doi.org/10.1007/s00382-003-0315-7

Craig, A., Valcke, S., & Coquart, L. (2017). Development and performance of a new version of the OASIS coupler, OASIS3-MCT_3.0. *Geoscientific Model Development*, *10*(9), 3297–3308. https://doi.org/10.5194/gmd-10-3297-2017

Dinezio, P. N., Puy, M., Thirumalai, K., Jin, F.-F., & Tierney, J. E. (2020). Emergence of an equatorial mode of climate variability in the Indian Ocean. *Science Advances*, *6*(19), eaay7684. https://doi.org/10.1126/sciadv.aay7684

EC-Earth Consortium (EC-Earth). (2019). EC-Earth-Consortium ECEarth3-LR model output prepared for CMIP6 CMIP piControl, Version 20200409. *Earth System Grid Federation*, https://doi.org/10.22033/ESGF/CMIP6.4847

EC-Earth Consortium (EC-Earth). (2020). EC-Earth-Consortium ECEarth3-LR model output prepared for CMIP6 PMIP lig127k, Version 20200409. *Earth System Grid Federation*, https://doi.org/10.22033/ESGF/CMIP6.4798

Gadgil, S., & Kumar, K. R. (2006). The Asian monsoon-agriculture and economy. In *The Asian monsoon* (pp. 651–683). Springer.

Goswami, B. N., Venugopal, V., Sengupta, D., Madhusoodanan, M., & Xavier, P. K. (2006). Increasing trend of extreme rain events over India in a warming environment. *Science*, *314*(5804), 1442–1445. https://doi.org/10.1126/science.1132027

Han, Z., Su, T., Zhang, Q., Wen, Q., & Feng, G. (2019). Thermodynamic and dynamic effects of increased moisture sources over the Tropical Indian Ocean in recent decades. *Climate Dynamics*, *53*(11), 7081–7096. https://doi.org/10.1007/s00382-019-04977-w

Harrison, S. P., Bartlein, P., Izumi, K., Li, G., Annan, J., Hargreaves, J., et al. (2015). Evaluation of CMIP5 palaeo-simulations to improve climate projections. *Nature Climate Change*, *5*(8), 735–743. https://doi.org/10.1038/nclimate2649

Hazeleger, W., Severijns, C., Semmler, T., Stefanescu, S., Yang, S., Wang, X., et al. (2010). EC-Earth: A seamless earth-system prediction approach in action. *Bulletin of the American Meteorological Society*, *91*(10), 1357–1363. https://doi.org/10.1175/2010BAMS2877.1

Hazeleger, W., Wang, X., Severijns, C., Ştefănescu, S., Bintanja, R., Sterl, A., et al. (2012). EC-Earth V2. 2: Description and validation of a new seamless earth system prediction model. *Climate Dynamics*, *39*(11), 2611–2629. https://doi.org/10.1007/s00382-011-1228-5

Hirabayashi, Y., Mahendran, R., Koirala, S., Konoshima, L., Yamazaki, D., Watanabe, S., et al. (2013). Global flood risk under climate change. *Nature Climate Change*, *3*(9), 816–821. https://doi.org/10.1038/NCLIMATE1911

Hoffman, J. S., Clark, P. U., Parnell, A. C., & He, F. (2017). Regional and global sea-surface temperatures during the last interglaciation. *Science*, *355*(6322), 276–279. https://doi.org/10.1126/science.aai8464

Joussaume, S., & Braconnot, P. (1997). Sensitivity of paleoclimate simulation results to season definitions. *Journal of Geophysical Research*, *102*(D2), 1943–1956. https://doi.org/10.1029/96JD01989

Kageyama, M., Braconnot, P., Harrison, S. P., Haywood, A. M., Jungclaus, J. H., Otto-Bliesner, B. L., et al. (2018). The PMIP4 contribution to CMIP6–Part 1: Overview and over-arching analysis plan. *Geoscientific Model Development*, *11*(3), 1033–1057. https://doi.org/10.5194/gmd-11-1033-2018

Kitoh, A., Endo, H., Krishna Kumar, K., Cavalcanti, I. F., Goswami, P., & Zhou, T. (2013). Monsoons in a changing world: A regional perspective in a global context. *Journal of Geophysical Research: Atmospheres*, *118*(8), 3053–3065. https://doi.org/10.1002/jgrd.50258

Li, J., Wu, Z., Jiang, Z., & He, J. (2010). Can global warming strengthen the East Asian summer monsoon? *Journal of Climate*, *23*(24), 6696–6705. https://doi.org/10.1175/2010JCLI3434.1

Li, J., & Zeng, Q. (2000). Significance of the normalized seasonality of wind field and its rationality for characterizing the monsoon. *Science in China Series D: Earth Sciences*, *43*(6), 646–653. https://doi.org/10.1007/BF02879509

Li, J., & Zeng, Q. (2002). A unified monsoon index. *Geophysical Research Letters*, *29*(8), 1274. https://doi.org/10.1029/2001GL013874

Li, T. (2018). False amount effect—A discussion on one issue of isotopic climatology. *Quaternary Sciences*, *38*(6), 1545–1548. https://doi.org/10.11928/j.issn.1001-7410.2018.06.20

Liu, G., Li, X., Chiang, H.-W., Cheng, H., Yuan, S., Chawchai, S., et al. (2020). On the glacial-interglacial variability of the Asian monsoon in speleothem $\delta^{18}O$ records. *Science Advances*, *6*(7), eaay8189. https://doi.org/10.1126/sciadv.aay8189

Lunt, D. J., Abe-Ouchi, A., Bakker, P., Berger, A., Braconnot, P., Charbit, S., et al. (2013). A multi-model assessment of last interglacial temperatures. *Climate of the Past*, *9*(2), 699–717. https://doi.org/10.5194/cp-9-699-2013

Madec, G. (2008). Note du Pôle modélisation, Inst. Pierre Simon Laplace (Vol. 27). *NEMO reference manual, ocean dynamic component: NEMO-OPAFr*. (Tech. Rep.,27).

Magiera, M., Lechleitner, F. A., Erhardt, A. M., Hartland, A., Kwiecien, O., Cheng, H., et al. (2019). Local and regional Indian summer monsoon precipitation dynamics during Termination II and the last interglacial. *Geophysical Research Letters*, *46*(21), 12454–12463. https://doi.org/10.1029/2019GL083721

Midhun, M., Lekshmy, P., Ramesh, R., Yoshimura, K., Sandeep, K., Kumar, S., et al. (2018). The effect of monsoon circulation on the stable isotopic composition of rainfall. *Journal of Geophysical Research: Atmospheres*, *123*, 5205–5221. https://doi.org/10.1029/2017JD027427

Montoya, M., von Storch, H., & Crowley, T. J. (2000). Climate simulation for 125 kyr BP with a coupled ocean–atmosphere general circulation model. *Journal of Climate*, *13*(6), 1057–1072. https://doi.org/10.1175/1520-0442(2000)013<1057:csfkbw>2.0.co;2

Otto-Bliesner, B. L., Braconnot, P., Harrison, S. P., Lunt, D. J., Abe-Ouchi, A., Albani, S., et al. (2017). The PMIP4 contribution to CMIP6–Part 2: Two interglacials, scientific objective and experimental design for Holocene and Last Interglacial simulations. *Geoscientific Model Development*, *10*(11), 3979–4003. https://doi.org/10.5194/gmd-10-3979-2017

Otto-Bliesner, B. L., Brady, E. C., Zhao, A., Brierley, C. M., Axford, Y., Capron, E., et al. (2021). Large-scale features of last interglacial climate: Results from evaluating the lig127k simulations for the coupled model intercomparison Project (CMIP6)-Paleoclimate Modeling intercomparison Project (PMIP4). *Climate of the Past*, *17*(1), 63–94. https://doi.org/10.5194/cp-17-63-2021

Ramesh, K., & Goswami, P. (2007). Reduction in temporal and spatial extent of the Indian summer monsoon. *Geophysical Research Letters*, *34*, L23704. https://doi.org/10.1029/2007GL031613

Roxy, M. K., Ritika, K., Terray, P., Murtugudde, R., Ashok, K., & Goswami, B. (2015). Drying of Indian subcontinent by rapid Indian Ocean warming and a weakening land-sea thermal gradient. *Nature Communications*, *6*(1), 1–10. https://doi.org/10.1038/ncomms8423

Saha, A., Ghosh, S., Sahana, A. S., & Rao, E. P. (2014). Failure of CMIP5 climate models in simulating post-1950 decreasing trend of Indian monsoon. *Geophysical Research Letters*, *41*(20), 7323–7330. https://doi.org/10.1002/2014GL061573

Saji, N., Goswami, B., Vinayachandran, P., & Yamagata, T. (1999). A dipole mode in the tropical Indian Ocean. *Nature*, *401*(6751), 360–363. https://doi.org/10.1038/43854

Salzmann, M., & Cherian, R. (2015). On the enhancement of the Indian summer monsoon drying by Pacific multidecadal variability during the latter half of the twentieth century. *Journal of Geophysical Research: Atmospheres*, *120*, 9103–9118. https://doi.org/10.1002/2015JD023313

Salzmann, M., Weser, H., & Cherian, R. (2014). Robust response of Asian summer monsoon to anthropogenic aerosols in CMIP5 models. *Journal of Geophysical Research: Atmospheres*, *119*, 11321–11337. https://doi.org/10.1002/2014JD021783

Scussolini, P., Bakker, P., Guo, C., Stepanek, C., Zhang, Q., Braconnot, P., et al. (2019). Agreement between reconstructed and modeled boreal precipitation of the Last Interglacial. *Science Advances*, *5*(11), eaax7047. https://doi.org/10.1126/sciadv.aax7047

Singh, D., Tsiang, M., Rajaratnam, B., & Diffenbaugh, N. S. (2014). Observed changes in extreme wet and dry spells during the South Asian summer monsoon season. *Nature Climate Change*, *4*(6), 456–461. https://doi.org/10.1038/nclimate2208

Sudharsan, N., Karmakar, S., Fowler, H. J., & Hari, V. (2020). Large-scale dynamics have greater role than thermodynamics in driving precipitation extremes over India. *Climate Dynamics*, *55*(9), 2603–2614. https://doi.org/10.1007/s00382-020-05410-3

Tan, M. (2014). Circulation effect: Response of precipitation $\delta^{18}O$ to the ENSO cycle in monsoon regions of China. *Climate Dynamics*, *42*(3–4), 1067–1077. https://doi.org/10.1007/s00382-013-1732-x

Terray, P., Sooraj, K., Masson, S., & Prodhomme, C. (2021). Anatomy of the Indian summer monsoon and ENSO relationships in state-of-the-art CGCMs: Role of the tropical Indian Ocean. *Climate Dynamics*, *56*(1), 329–356. https://doi.org/10.1007/s00382-020-05484-z

Tokinaga, H., Xie, S.-P., Deser, C., Kosaka, Y., & Okumura, Y. M. (2012). Slowdown of the Walker circulation driven by tropical Indo-Pacific warming. *Nature*, *491*(7424), 439–443. https://doi.org/10.1038/nature11576

Turner, A. G., & Annamalai, H. (2012). Climate change and the South Asian summer monsoon. *Nature Climate Change*, *2*(8), 587–595. https://doi.org/10.1038/nclimate1495

Turney, C. S., Jones, R. T., McKay, N. P., Van Sebille, E., Thomas, Z. A., Hillenbrand, C.-D., & Fogwill, C. J. (2020). A global mean sea surface temperature dataset for the Last Interglacial (129–116 ka) and contribution of thermal expansion to sea level change. *Earth System Science Data*, *12*(4), 3341–3356. https://doi.org/10.5194/essd-12-3341-2020

Vancoppenolle, M., Bouillon, S., Fichefet, T., Goosse, H., Lecomte, O., Morales Maqueda, M., & Madec, G. (2012). *The Louvain-la-Neuve sea ice model*. Notes du pole de modélisation, Institut Pierre-Simon Laplace (IPSL).

Vittal, H., Karmakar, S., Ghosh, S., & Murtugudde, R. (2020). A comprehensive India-wide social vulnerability analysis: Highlighting its influence on hydro-climatic risk. *Environmental Research Letters*, *15*(1), 014005. https://doi.org/10.1088/1748-9326/ab6499

Wang, B., Wu, Z., Li, J., Liu, J., Chang, C.-P., Ding, Y., & Wu, G. (2008a). How to measure the strength of the East Asian summer monsoon. *Journal of Climate*, *21*(17), 4449–4463. https://doi.org/10.1175/2008JCLI2183.1

Wang, Y., Cheng, H., Edwards, R. L., Kong, X., Shao, X., Chen, S., et al. (2008b). Millennial-and orbital-scale changes in the East Asian monsoon over the past 224,000 years. *Nature*, *451*(7182), 1090–1093. https://doi.org/10.1038/nature06692

Wu, G., Liu, Y., He, B., Bao, Q., Duan, A., & Jin, F.-F. (2012). Thermal controls on the Asian summer monsoon. *Scientific Reports*, *2*(1), 1–7. https://doi.org/10.1038/srep00404

Yeung, K. H., Menviel, L., Meissner, K. J., Taschetto, A. S., Ziehn, T., & Chamberlain, M. (2021). Land–sea temperature contrasts at the Last Interglacial and their impact on the hydrological cycle. *Climate of the Past*, *17*(2), 869–885. https://doi.org/10.5194/cp-17-869-2021

Zhang, Q., Berntell, E., Axelsson, J., Chen, J., Han, Z., de Nooijer, W., et al. (2021). Simulating the mid-Holocene, last interglacial and mid-Pliocene climate with EC-Earth3-LR. *Geoscientific Model Development*, *14*(2), 1147–1169. https://doi.org/10.5194/gmd-14-1147-2021

Zhang, Q., & Chen, J. (2020). Enhanced East Asian summer monsoon precipitation due to vegetation feedback during the last interglacial 127ka. *Quaternary Sciences*, *40*(6), 1499–1512. https://doi.org/10.11928/j.issn.1001-7410.2020.06.11

Zhang, Y., Li, J., Xue, J., Feng, J., Wang, Q., Xu, Y., et al. (2018). Impact of the South China sea summer monsoon on the Indian Ocean dipole. *Journal of Climate*, *31*(16), 6557–6573. https://doi.org/10.1175/JCLI-D-17-0815.1